Flat Bands and Wigner Crystallization in the Honeycomb Optical Lattice

Congjun Wu,[1,2] Doron Bergman,[3] Leon Balents,[3] and S. Das Sarma[4]

[1]*Kavli Institute for Theoretical Physics, University of California, Santa Barbara, California 93106, USA*
[2]*Department of Physics, University of California, San Diego, California 92093, USA*
[3]*Department of Physics, University of California, Santa Barbara, California 93106, USA*
[4]*Condensed Matter Theory Center, Department of Physics, University of Maryland, College Park, Maryland 20742, USA*
(Received 8 February 2007; published 16 August 2007)

We study the ground states of cold atoms in the tight-binding bands built from p orbitals on a two dimensional honeycomb optical lattice. The band structure includes two completely flat bands. Exact many-body ground states with on-site repulsion can be found at low particle densities, for both fermions and bosons. We find crystalline order at $n = \frac{1}{6}$ with a $\sqrt{3} \times \sqrt{3}$ structure breaking a number of discrete lattice symmetries. In fermionic systems, if the repulsion is strong enough, we find the bonding strength becomes *dimerized* at $n = \frac{1}{2}$. Experimental signatures of crystalline order can be detected through the noise correlations in time of flight experiments.

DOI: 10.1103/PhysRevLett.99.070401 PACS numbers: 05.30.Fk, 03.75.Nt, 03.75.Ss, 05.50.+q

Optical lattices have opened up a new venue in which to study strongly correlated systems, with the possibility of precisely controlled interactions. For example, the superfluid–Mott-insulator transition [1] for bosons has been observed. Many interesting states with novel magnetic and superfluid properties in optical lattices have also been proposed by using high-spin bosons and fermions [2]. In addition, optical lattices provide the opportunity for studying another important aspect of strongly correlated systems, orbital physics, which plays an important role in metal-insulator transitions, superconductivity, and colossal magnetoresistance [3].

Cold atom systems with orbital degrees of freedom exhibit new features which are not usually realized in solid state systems. Recently, the properties of the bosons in the first excited p-orbital bands have attracted a great deal of theoretical attention [4–9], including predictions of a nematic superfluid state [5], antiferromagnetic ordering of orbital angular momentum (OAM) [6,7], a striped phase of OAM in the triangular lattice [8], and a bond algebraic liquid phase [9]. Experiments carried out by Browaeys *et al.* [10] and Köhl *et al.* [11] have demonstrated the population of higher orbital bands in both bosons and fermions. Recently, Fölling *et al.* have showed the existence of both the Mott-insulating and superfluid states of the p-band bosons [12].

The physics of graphene captured by the 2D honeycomb lattice has generated tremendous interest as a realization of Dirac fermions [13]. In graphene, the active bands near the Fermi energy are "π" type, composed of the p_z orbitals directly normal to the graphene plane. The other two p orbitals ($p_{x,y}$) lie in-plane, and exhibit both orbital degeneracy and spatial anisotropy. However, they hybridize with the s band and the resulting σ-bonding band is completely filled. In contrast, in optical lattices, $p_{x,y}$ bands are well separated from the s band with negligible hybridization, giving rise to the possibility of interesting new physics. The honeycomb optical lattice has already been realized quite some time ago, by using three coplanar laser beams [14].

In this Letter, we study the $p_{x,y}$-orbital physics in the 2D honeycomb lattice. We find the lowest energy band is *completely* flat over the entire Brillouin zone (BZ). When the flat band is partially filled, the effects of interactions are entirely nonperturbative. For sufficient low densities the ground states are "Wigner" crystals (we slightly abuse this nomenclature to apply it generally to both bosons and fermions). We obtain the *exact* many-body plaquette Wigner-crystal state at filling $\langle n \rangle = \frac{1}{6}$. For fermionic systems, we obtain additional crystalline ordered states at higher commensurate fillings. The noise correlation in the time of flight image should detect the order in these states.

We first discuss the single-particle spectrum. The optical potential on each site is approximated by a 3D anisotropic harmonic well with frequencies $\omega_z \gg \omega_x = \omega_y = \omega_{xy}$, and thus the p_z orbital is well separated in energy from the $p_{x,y}$ orbitals. Since the honeycomb lattice is bipartite, we denote by A and B its two sublattices. We define three unit vectors $\hat{e}_{1,2} = \pm\frac{\sqrt{3}}{2}\hat{e}_x + \frac{1}{2}\hat{e}_y$, $\hat{e}_3 = -\hat{e}_y$ pointing from each A site to its three B neighbors. The projection of the p-orbitals along the three $\hat{e}_{i=1,2,3}$ directions are defined as $p_i \equiv (p_x\hat{e}_x + p_y\hat{e}_y)\cdot\hat{e}_i$. Only two of them are linearly independent. The kinetic energy reads

$$H_0 = t_{\parallel} \sum_{\vec{r}\in A, i=1-3} \{p^{\dagger}_{\vec{r},i} p_{\vec{r}+a\hat{e}_i,i} + \text{H.c.}\} - \mu \sum_{\vec{r}\in A\oplus B} n_{\vec{r}}, \quad (1)$$

where the σ-bonding term $t_{\parallel}$ describes the hopping between p orbitals on neighboring sites parallel to the bond direction, a is the nearest neighbor distance, and $n_{\vec{r}} = n_{\vec{r},x} + n_{\vec{r},y}$ is the total particle number in both p_x and p_y orbitals at the site $\vec{r}$. $t_{\parallel}$ is positive due to the odd parity of the p orbitals and is set to 1 below. Equation (1) neglects the π-bonding $t_{\perp}$ which describes the hopping between p orbitals perpendicular to the bond direction. Typically

 © 2007 The American Physical Society

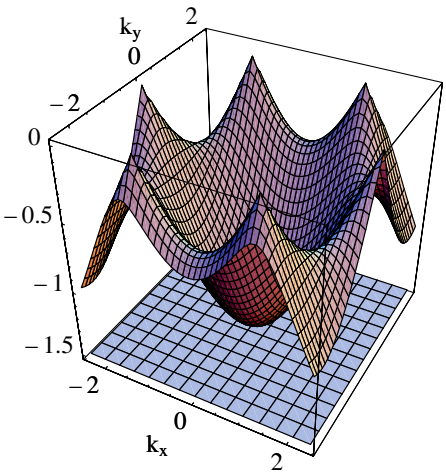

FIG. 1 (color online). Dispersion of the two-lowest $p_{x,y}$-orbital bands $E_{1,2}$. The band E_1 is completely flat, while E_2 exhibits Dirac points at $K_{1,2} = (\pm\frac{4\pi}{3\sqrt{3}a}, 0)$. The other two bands are symmetric with respect to $E = 0$.

$t_\parallel/t_\perp \gg 1$ due to the high spatial anisotropy of the p orbitals. We have numerically confirmed this for the optical potential realized in experiment $V(\vec{r}) = V_0\sum_{i=1-3}\cos(\vec{p}_i\cdot\vec{r})$, where $\vec{p}_i = p_0\hat{e}_i$ and $p_0 = \frac{4\pi}{3a}$ [14]. Namely, $t_\perp \approx 0.02t_\parallel$ and $t_\parallel \approx 0.24E_R$ at $V_0/E_R = 5$ (E_R is the recoil energy).

The band structure contains both flat bands and Dirac cones. Each unit cell consists of two sites, each of which contains two orbitals $p_{x,y}$, resulting in four bands. The BZ takes the shape of a regular hexagon with edge length $4\pi/(3\sqrt{3}a)$. The dispersion of all the bands is symmetric with respect to the zero energy because of the bipartite nature of the lattice. The band structure consists of $E_{1,4}(\vec{k}) = \mp\frac{3}{2}$, $E_{2,3}(\vec{k}) = \mp\frac{1}{2}\sqrt{3 + 2\sum_i \cos\vec{k}\cdot\vec{b}_i}$, where $\vec{b}_1 = a(\hat{e}_2 - \hat{e}_3)$, $\vec{b}_2 = a(\hat{e}_3 - \hat{e}_1)$, and $\vec{b}_3 = a(\hat{e}_1 - \hat{e}_2)$. We show only the two lowest bands $E_{1,2}$ in Fig. 1, which touch at the Brillouin zone center. The bottom and top bands turn out to be completely flat. The two middle bands are dispersive with a width determined by $t_\parallel$, which are the same as in graphene with two nonequivalent Dirac points located at $\vec{K}_{1,2} = (\pm\frac{4\pi}{3\sqrt{3}a}, 0)$. We will not repeat the extensively studied Dirac cone physics here, but rather focus on the new features brought by the flat bands instead.

The degeneracy of all momentum eigenstates in the flat bands allows us to take any superposition of these states, and, in particular, to construct eigenstates that are *localized*. As depicted in Fig. 2(a), for each hexagon plaquette $\vec{R}$, there exists one such eigenstate for the bottom band

$$|\psi_{\vec{R}}\rangle = \sum_{j=1}^{6}(-1)^{j-1}\{\cos\theta_j|p_{j,x}\rangle - \sin\theta_j|p_{j,y}\rangle\} \qquad (2)$$

where j is the site index and $\theta_j = (j-1)\frac{\pi}{3}$. The orbital configuration on each site is perpendicular to the links external to the hexagonal loop. This orbital orientation, together with destructive interference of hopping amplitudes, prevent the particle from "leaking" off of the plaquette. The states $|\psi_{\vec{R}}\rangle$ are all linearly independent apart from one constraint $\sum_{\vec{R}}|\psi_{\vec{R}}\rangle = 0$ under periodic boundary conditions. The Bloch wave states are constructed as $|\psi_k\rangle_1 = \frac{1}{\sqrt{N_k}}\sum_k e^{i\vec{k}\cdot\vec{R}}|\psi_{\vec{R}}\rangle[\vec{k} \neq (0,0)]$, with the normalization factor $N_k = \frac{8}{3}(3 - \sum_i \cos\vec{k}\cdot\vec{b}_i)$. The doubly degenerate eigenstate at $\vec{k} = (0,0)$ cannot be constructed from the above plaquette states. They are $|\psi_{\vec{k}=(0,0)}\rangle_{1,2} = \sum_{\vec{r}\in A}|p_{x(y),\vec{r}}\rangle - \sum_{\vec{r}\in B}|p_{x(y),\vec{r}}\rangle$.

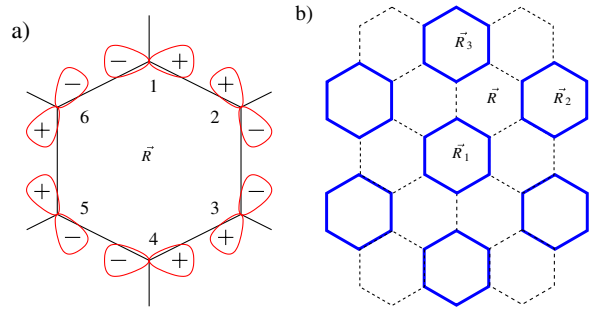

FIG. 2 (color online). (a) The Wannier-like localized eigenstate for the lowest band. The orbital configuration at each site is oriented along a direction tangential to the closed loop on which the particle is delocalized. (b) The configuration of the close-packed Wigner-crystal state for both bosons and fermions at $n = 1/6$. Each thickened plaquette has the same configuration as in (a).

Because of the orbital degeneracy, the on-site interaction for spinless fermions remains Hubbard-like as

$$H_{\rm int} = U\sum_{\vec{r}} n_{\vec{r},x}n_{\vec{r},y}. \qquad (3)$$

In order to enhance U between neutral atoms, we may use the ^{53}Cr atom which has a large magnetic moment of $6\mu_B$ (Bohr magneton), and polarize the spin with an external magnetic field. The length scale of p_{xy} orbitals $l_{x,y} = \sqrt{\hbar/m\omega_{x,y}}$ is typically one order smaller than a. For example, we estimate that $l_{x,y}/a \approx 0.2$ at $V_0/E_R = 5$. Assuming strong confinement in the z axis $l_z \ll l_{x,y}$, the vector linking two atoms in p_x and p_y orbits almost lies in the plane. U can be adjusted from repulsive to attractive by tuning the polarization direction from perpendicular to parallel to the xy plane. We will only discuss repulsive U below. We estimate that U can easily reach the order of E_R which is much larger than $t_\parallel$. The off-site interactions are small and decay with distance as $1/r^3$, and thus are neglected. For example, the nearest neighbor interaction is at the order of $(\frac{l_{x,y}}{a})^3U \approx 10^{-2}U$. The on-site interaction for p-band bosons is given in Ref. [6,8].

When the flat band is partially filled, the effect of interactions is nonperturbative. At sufficiently low particle density $n \leq 1/6$, both the interactions and the kinetic energy can be minimized simultaneously. This can be realized if the individual particles localize into the plaquette states depicted in Fig. 2(a). These are exact eigen-

states of the flat band, and therefore minimize kinetic energy. Any arrangement of the plaquette states where they do not overlap will cost no interaction energy. These localized plaquette states therefore constitute *exact* many-body ground states. The maximum density (close-packed) arrangement of nonoverlapping plaquettes has filling $n = 1/6$, and has the structure depicted in Fig. 2(b). The $\sqrt{3} \times \sqrt{3}$ structure breaks the lattice translation symmetry and is threefold degenerate. At zero temperature, the particle density *jumps* from 0 to 1/6 as the chemical potential is increased through $\mu = -3/2$. Similar flat band behavior has been studied in the magnon spectra of a number of frustrated magnets in a large magnetic field [15] near full polarization of the magnet. The degenerate states for the Kagome antiferromagnet are in exact one to one correspondence to those of our model. Thus the two models have identical thermodynamics (if fluctuations are restricted to these states, as appropriate for $k_B T \ll t_\parallel, U$). This is described by the classical hard hexagon model [15], which exhibits a second order thermal phase transition in the 3-state Potts model universality class, breaking translational symmetry, when the fugacity of the hexagon $z_c = (11 + \sqrt{5})/2$. In this state, the atoms do not touch each other, thus particle statistics do not play any role. The Wigner crystal is also expected to appear for bosons in this optical lattice at filling $n = \frac{1}{6}$. In contrast, Wigner crystal is not possible in graphene systems [16].

When the filling $n > 1/6$, exact solutions are no longer available for the interacting Hamiltonian. For simplicity, in this regime we shall only discuss the case of spinless fermions, within a mean-field treatment. We decouple Eq. (3) in both the direct and exchange channels as

$$H_{mf,\mathrm{int}} = \frac{U}{2} \sum_{\vec{r} \in A \oplus B} \{ n_{\vec{r},x}[\langle n_{\vec{r}} \rangle - \langle n_{\vec{r},3} \rangle] + n_{\vec{r},y}[\langle n_{\vec{r}} \rangle + \langle n_{\vec{r},3} \rangle] - p^\dagger_{\vec{r}x} p_{\vec{r}y}[\langle n_{\vec{r},1} \rangle - i \langle n_{\vec{r},2} \rangle] - \mathrm{H.c.} \}, \tag{4}$$

and solve it self-consistently. Here $n_{1,2,3}$ are the pseudospin operators defined as $n_{\vec{r},3} = \frac{1}{2}(p^\dagger_{\vec{r}x} p_{\vec{r}x} - p^\dagger_{\vec{r}y} p_{\vec{r}y})$, $n_{\vec{r},1} = \frac{1}{2} \times (p^\dagger_{\vec{r}x} p_{\vec{r}y} + \mathrm{H.c.})$, $n_{\vec{r},2} = \frac{1}{2i}(p^\dagger_{\vec{r}x} p_{\vec{r}y} - \mathrm{H.c.})$. The $n_{\vec{r},1}, n_{\vec{r},3}$ operators are time-reversal invariant, and describe the preferential occupation of a "dumbbell-shaped" real p-orbital orientation; $n_{\vec{r},2}$ is the orbital angular momentum, and is time-reversal odd. At the mean-field level $\langle n_{\vec{r},2} \rangle$ is zero. In order to obtain the plaquette order in Fig. 2, we take the six sites around a plaquette as one enlarged unit cell in the mean-field calculation.

The numerically determined phase boundary between the 1/6 state and a compressible phase at higher density is shown in Fig. 3. The charge gap grows roughly linearly with U in the weak interaction regime, and saturates at a value comparable to $t_\parallel$ in the strong interaction regime. This can be understood as follows: in the weak interaction case, we choose a plaquette $\vec{R}$ which is adjacent to three occupied plaquettes $\vec{R}_{1,2,3}$ as depicted in Fig. 2(b), and put an extra particle in it. The cost of the repulsion is $\frac{U}{6}$. In the strong coupling case, we put the particle into an excited state of the occupied plaquette $\vec{R}_1$ while fixing the orbital configuration on each site. Because fermions are spinless, the cost of energy comes from the kinetic part with the value of $\frac{3}{4} t_\parallel$. Thus the charge gap is $\Delta < \min(\frac{1}{6} U, \frac{3}{4} t_\parallel)$ which agrees with the numeric result.

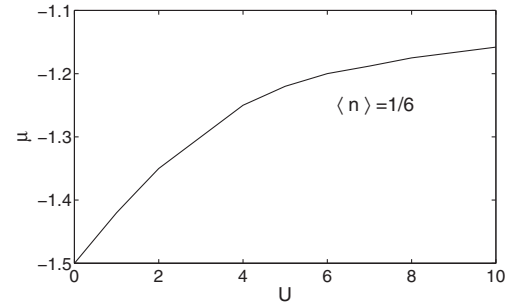

FIG. 3. The phase boundary of the incompressible plaquette Wigner-crystal state of spinless fermions at $\langle n \rangle = \frac{1}{6}$.

The curves of the filling n vs μ in both the weak and strong coupling regimes are depicted in Fig. 4. In both cases, the plaquette Wigner state appears as a plateau with $\langle n \rangle = \frac{1}{6}$. In the weak coupling regime ($U/t_\parallel = 1$), as μ passes the charge gap, $\langle n \rangle$ increases quickly corresponding to filling up other states in the flat band. Because of the background crystal ordering, those states are no longer degenerate, but develop weak dispersion. A significant reduction in the density of states (DOS) occurs at the approximately commensurate filling of $\langle n \rangle \approx \frac{1}{3}$, but it is not a strict plateau. At $\langle n \rangle > 1/2$, after the flat band is completely filled, the interaction effects are no longer important. Near half-filling, the DOS vanishes where the physics is dominated by the Dirac cones.

The physics changes dramatically in the strong coupling regime. We looked specifically at ($U/t = 10$), where we found a series of plateaus appear at commensurate fillings $\langle n \rangle = \frac{i}{6}$ ($i = 1$–6). The large charge gap at $\langle n \rangle = 1$ is of the order of U. The other plateaus with $\langle n \rangle < 1$ are the novel features the p-orbital model presents. In addition to the plaquette bond order at $\langle n \rangle = \frac{1}{6}$ discussed above, rich structures including dimer and trimer bond orders appear at other plateaus with $\langle n \rangle < 1$. We will present these patterns in detail in a future publication. Here a dimer refers to a superposition of the two states of two sites where one is occupied, while the other is empty. The dimerized state at $\langle n \rangle = \frac{1}{2}$ is illustrated in Fig. 5. Each dimer is represented as a thickened bond where the orbital configuration is along the bond. We check that the bonding energy for the thickened bond is approximately $0.95 t_\parallel$ at $U/t_\parallel = 10$ which is about one order larger than that of other bonds.

Next we discuss the effect of adding a small π-hopping $t_\perp$ term. Then the lowest energy band acquires weak dispersion, with a small band width of $t_\perp$. This associated kinetic energy cost for the $n = \frac{1}{6}$ plaquette state is of order $t_\perp$ per particle. A stability condition of this state can

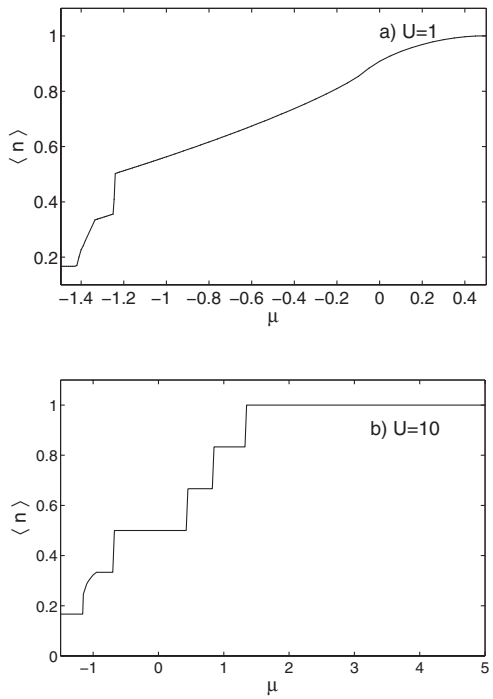

FIG. 4. The filling $\langle n \rangle$ vs the chemical potential μ for spinless fermions for weak (a) and strong (b) interactions. Because of particle-hole symmetry, only the part with μ from the band bottom $-\frac{3}{2}t_{\parallel}$ to $U/2$ is shown. Only one plateau appears in (a) at $n = \frac{1}{6}$, while a series of plateaus appear in (b) at $n = 1/6$, $1/3$, $1/2$, $2/3$, $5/6$, and 1.

therefore be roughly estimated as $\frac{U}{6} > t_{\perp}$. We have checked numerically that the $\frac{1}{6}$-plateau survives at $U > t_{\parallel}$ with the value of $t_{\perp} = 0.1t_{\parallel}$. Other plateaus appearing in the strong coupling regime are not sensitive to small $t_{\perp}$.

The plaquette Wigner-crystal phase in Fig. 2(b) should manifest itself in the noise correlation for the time of flight (TOF) signals. In the presence of the plaquette order, the reciprocal lattice vector for the enlarged unit cell becomes $\vec{G}_1 = (\frac{4\pi}{3\sqrt{3}a}, 0)$ and $\vec{G}_2 = (\frac{-2\pi}{3\sqrt{3}a}, \frac{2\pi}{3a})$. The correlation function is defined as $C_t(\vec{r}, \vec{r}') = \langle n(\vec{r})n(\vec{r}')\rangle_t - \langle n(\vec{r})\rangle_t \langle n(\vec{r}')\rangle_t$. After a spatial averaging and normalization, we find

$$C_t(\vec{d}) = \int d\vec{r} \frac{C_t(\vec{r} + \frac{\vec{d}}{2}, \vec{r} - \frac{\vec{d}}{2})}{\langle n(\vec{r} + \frac{\vec{d}}{2})\rangle_t \langle n(\vec{r} - \frac{\vec{d}}{2})\rangle_t} \propto \pm \sum_{\vec{G}} \delta(\vec{k} - \vec{G}), \tag{5}$$

where $+$ ($-$) is for bosons (fermions), respectively, $\vec{k} = m\vec{d}/(\hbar t)$, and $\vec{G} = m\vec{G}_1 + n\vec{G}_2$ with m, n integers.

There are numerous directions open for further exploration. Some interesting variations on the model are to consider *spinful* fermions, for which there is a possibility of ferromagnetism as a result of the flat bands, or attractive interactions, in which pairing and the BCS-Bose-Einstein condensation crossover in the flat band might prove interesting. Most intriguing is the possibility of exotic incompressible states analogous to the Laughlin liquid in the fractional quantum-Hall effect (FQHE). These cannot be

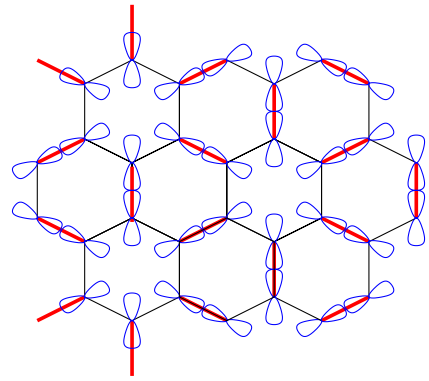

FIG. 5 (color online). The dimerized state of spinless fermions with filling $\langle n \rangle = \frac{1}{2}$. Each thickened (red) bond corresponds a dimer containing one particle.

captured within the mean-field approximation used here for $n > 1/6$. If one could devise appropriate variational liquid states projected into the flat band, these could be compared energetically with the Wigner crystals found here. Given the richness and surprises encountered in the FQHE, flat band physics in optical lattices appears rife with possibility. The comparison with the fermion condensation where the flat band arises due to strong interactions will also be interesting [17].

C. W. thanks helpful discussions with A. Carlsson, L. M. Duan, and Z. Nussinov. C. W. is supported by the NSF No. Phy99-07949. D. B. and L. B. are supported by No. NSF-DMR-04-57440 and the Packard foundation. S. D. S. is supported by LPS-NSA and ARO-DTO.

[1] M. Greiner *et al.*, Nature (London) **415**, 39 (2002).
[2] E. Demler *et al.*, Phys. Rev. Lett. **88**, 163001 (2002); F. Zhou *et al.*, Phys. Rev. Lett. **87**, 080401 (2001); C. Wu *et al.*, Phys. Rev. Lett. **91**, 186402 (2003); C. Wu, Phys. Rev. Lett. **95**, 266404 (2005); C. Wu, Mod. Phys. Lett. B **20**, 1707 (2006).
[3] Y. Tokura and N. Nagaosa, Science **288**, 462 (2000).
[4] V. W. Scarola *et al.*, Phys. Rev. Lett. **95**, 033003 (2005).
[5] A. Isacsson *et al.*, Phys. Rev. A **72**, 053604 (2005).
[6] W. V. Liu and C. Wu, Phys. Rev. A **74**, 013607 (2006).
[7] A. B. Kuklov, Phys. Rev. Lett. **97**, 110405 (2006).
[8] C. Wu *et al.*, Phys. Rev. Lett. **97**, 190406 (2006).
[9] C. Xu and M. P. A. Fisher, arXiv:cond-mat/0611602.
[10] A. Browaeys *et al.*, Phys. Rev. A **72**, 053605 (2005).
[11] M. Köhl *et al.*, Phys. Rev. Lett. **94**, 080403 (2005).
[12] T. Mueller *et al.*, arXiv:0704.2856.
[13] K. S. Novoselov *et al.*, Nature (London) **438**, 197 (2005); Y. Zhang *et al.*, Nature (London) **438**, 201 (2005).
[14] G. Grynberg, Phys. Rev. Lett. **70**, 2249 (1993).
[15] J. Schulenburg *et al.*, Phys. Rev. Lett. **88**, 167207 (2002); M. E. Zhitomirsky and H. Tsunetsugu, Prog. Theor. Phys. Suppl. **160**, 361 (2005); J. Schnack and O. Derzhko *et al.*, arXiv:cond-mat/0612281.
[16] H. P. Dahal *et al.*, Phys. Rev. B **74**, 233405 (2006).
[17] V. A. Khodel *et al.*, JETP Lett. **51**, 553 (1990).